

Reference

NBS
PUBLICATIONS



NBSIR 85-2997

Estimation of Power-Law Creep Parameters from Bend Test Data

Tze-jeer Chuang

U.S. DEPARTMENT OF COMMERCE
National Bureau of Standards
Center for Materials Science
Inorganic Materials Division
Gaithersburg, MD 20899

February 1985

NBS-DOE-Contract No. DE-A105-80OR20679

NBS-AFOSR-ISSA-84-00013

Prepared for
Department of Energy
AR&TD Fossil Energy Materials Program
Washington, DC

and

Air Force
Office of Scientific Research
Washington, DC

QC
100
.U56
35-2997
1985

NBSIR 85-2997

**ESTIMATION OF POWER-LAW CREEP
PARAMETERS FROM BEND TEST DATA**

Ref-NBS
QC100
.456
NO.85-2997
1985

Tze-jeer Chuang

U.S. DEPARTMENT OF COMMERCE
National Bureau of Standards
Center for Materials Science
Inorganic Materials Division
Gaithersburg, MD 20899

February 1985

NBS-DOE-Contract No. DE-A105-800R20679

NBS-AFOSR-ISSA-84-00013

Prepared for
Department of Energy
AR&TD Fossil Energy Materials Program
Washington, DC

and

U.S. Air Force
Office of Scientific Research
Washington, DC



U.S. DEPARTMENT OF COMMERCE, Malcolm Baldrige, *Secretary*
NATIONAL BUREAU OF STANDARDS, Ernest Ambler, *Director*

ESTIMATION OF POWER-LAW CREEP PARAMETERS FROM BEND TEST DATA

by

Tze-jeer Chuang
Center for Materials Science
National Bureau of Standards
Gaithersburg, MD 20899

ABSTRACT

Power-law creep parameters of brittle ceramic materials are commonly deduced from load-point displacement data generated by four-point bend experiments, under the assumption that tensile and compressive behaviors obey the same constitutive law. However, because of microcracking and cavitation, it is now well recognized that this premise may not always be valid. The present paper presents an analysis which takes the differences into account. Governing equations are first derived for the location of the neutral axis of a beam under bending which does not in general pass through the centroid of the cross section and for the creep response in terms of both curvature rate and load-point displacement rate as functions of the applied moment and power-law creep parameters. Numerical solutions are obtained for any given set of material constants over a wide range of applied moments. It is shown from the plots of creep response versus applied moment on a logarithmic scale that even linear curves over a narrow range of applied moment do not necessarily imply identical stress exponents and that nonlinear curves concave upward signify a profound difference in stress exponent between tension and compression. An example of applying the present analysis to a set of load-point displacement data on glass-alumina beam specimens crept at 1100°C is given. The results show that the conventional method over/underestimates the creep rates in compression/tension by two orders of magnitude, indicating a need of using the more accurate analysis presented here. Several recommendations are offered to improve the estimation of power-law creep parameters from bend test data.

1. Introduction

The present paper is concerned with steady-state creep deformation behavior of structural ceramics which are candidate materials for high-temperature stress-bearing applications, and aims at developing a mathematical scheme from which individual tensile and compressive power-law creep parameters can be estimated from conventional four-point bend test measurements. Instead of directly relying on uniaxial testing, flexural test methods are frequently adopted as an alternative to generate data from which information on materials' creep behavior may be extracted (see for example [1-2]). This practice can be attributed to the fact that a bending experiment is more stable and easier to perform without involving problems of fixturing and alignment usually associated with tension testing of brittle materials at high temperatures. A challenging issue that must be resolved for a given set of data produced from crept bend bars is: how can one, if possible, accurately estimate the uniaxial creep behavior (both in tension and in compression) when the applied stress is given? Since bending data contain both tensile and compressive components, it is perhaps natural to expect that the resulting predictions would be strongly influenced by the form of constitutive equations assumed a priori.

Extensive literature review on the thermal creep of ceramics [3] indicates that generally speaking the steady-state behavior relating creep strain rate $\dot{\epsilon}_s$ to applied stress σ can be described by Norton's law in a form $\dot{\epsilon}_s = A \sigma^n$, where A is pre-exponent constant depending only on test temperature and material's properties; n is stress exponent which may or

may not depend on stress. Hollenberg, et al. [4] presented the first analysis in which stresses and strains in the crept beam specimens can be calculated from the bend test data provided tensile power-law creep behaves identically to its compressive counterpart. This simplifies the analytical work substantially and allows the solutions to be presented in closed forms as the neutral axis location in this case always coincides with the center line of the beam height regardless of the magnitude of the applied loads.

However, it is now well recognized that tensile response might be distinct from its compressive counterpart inside a beam for a given material even tested under identical environments (see for example [5-6]). Consequently, for application to plain concrete, Krajcinovic [7] developed a damage theory for beams under pure bending in order to justify that tensile stresses assume a parabolic distribution in terms of strain while the compression behavior remains linearly elastic obeying Hook's law. More recently, Rosenfield et al. [8] extended this time-independent analysis to two more constitutive equations in tension, namely linear elastic with lower effective Young's modulus and elastic-perfectly plastic while once again leaving the compressive portion unchanged. On the other hand, within the arena of power-law creep, Finnie [9] was the first to recognize the possible situation of pronounced differences between tensile and compressive creep. His analysis permits $A_t \neq A_c$ and is capable of predicting creep rates from data generated by creep bending of a trapezoidal cross section beam provided n_t and n_c are of unity; here subscripts t and c refer to the cases of tension and compression

respectively. Talty and Dirks [10] extended the analysis of the same trapezoidal beam to a more general case of N other than unity (i.e. $n_t = n_c = N$).

The present paper extends the previous work to a completely general case of unequal tension vs compression power-law creep behaviors wherein not only the pre-exponent factors are permitted to be distinctive ($A_t \neq A_c$) but also the stress exponent constants may be unequal ($n_t \neq n_c$). For the sake of simplicity, only rectangular beams of uniform cross-sections are considered. Further, the existence of a steady-state is assumed so that time can be eliminated as a variable in the study. This assumption requires that the transient stage be short-lived and thus can be ignored, although it should be acknowledged that this phenomenon may sometimes become important [11-12] when a well-defined steady state does not develop [13].

In the next section, governing equations are first derived which relate separately the position of neutral axis and the applied moment to the curvature rate, \dot{K} and (unknown, a priori) power-law creep parameters. Computer programs were developed to solve these coupled non-linear algebraic equations numerically. Solutions are obtained in graphic form for an arbitrary set of power law constants. Graphic solutions are also given in terms of the load-point displacement rate, $\dot{\Delta}_p$ - a more measurable quantity than \dot{K} for collecting data on specimen's response. Cases of $n_t = n_c = N$ as examined by Talty and Dirks [10] and $A_t = A_c = A$, $n_t = n_c = N$ as analyzed by Hollenberg, et al. [4] are then presented as special cases of the present investigation. From the point of view of an experimenter,

in order to apply the current theory, a parametric study method must be used from which curves can be produced from the computer programs to match the discrete data points which are dictated by creep bend tests. Once accurate matching is achieved, the predicted power-law parameters become available at once from the well-fitted curve. For the sake of demonstration of how to use the theory, an example is given to estimate the four power-law constants from a set of six bend test data on debased alumina beams crept at 1100°C for a duration of more than 100 h. At conclusion, we are able to make some recommendations from the present analysis for those who prefer using the four-point bend test method to characterize power-law creep behavior in structural ceramics. Those suggestions should lead to more accurate characterization of creep properties.

2. Analysis

2.1 Derivation of the governing equations

In this section, we derive the control equations that relate material response to external variables and material constants, for a rectangular beam under four-point creep bending. (See Fig. 1)

As already discussed in the preceding section, under the action of some constant external loads the material is assumed to respond in the steady state according to a power law of the form:

$$\dot{\epsilon}_{sc} = A_c (\sigma/\sigma_0)^{n_c}, \quad \sigma \text{ in compression} \quad (1a)$$

and

$$\dot{\epsilon}_{st} = A_t (\sigma/\sigma_0)^{n_t}, \quad \sigma \text{ in tension} \quad (1b)$$

where $\dot{\epsilon}_s$ is steady-state creep strain rate; A and n are materials constant, σ is the normal stress and σ_0 is a reference stress. The subscript c and t refers to the case in compression and in tension respectively. A schematic sketch of Eq. 1 applied to a beam is given in Fig. 2.

The derivation that follows adopts the conventional simple beam theory which entails a fundamental assumption, known as Bernoulli's hypothesis, that planar sections remain plane during bending when creep is taking place so that no warping will occur (because of the need for geometric compatibility this condition seems to hold in practice [14]). This implies that the strain rate $\dot{\epsilon}$ of a fiber element is linearly dependent on Y, the distance away from the neutral axis where $\dot{\epsilon} = 0$ and the curvature rate, \dot{K} serves as a proportionality constant. Thus

$$\dot{\epsilon} = \dot{K} Y$$

and the stress distribution over the cross section of the beam is highly nonlinear and has the following form, according to Eq. (1):

$$\sigma(Y) = \sigma_0 \left(\frac{Y \dot{K}}{A} \right)^{1/n} \quad (2)$$

regardless of the sign of stress. Equilibrium requirements then dictate that the total force acting on the compression side of the cross-section be counter-balanced by its tensile counterpart. This means that $F_c = F_t$

or $B \int_0^{H_c} \sigma dY = B \int_0^{H_t} \sigma dY$ where B is the beam width and $H (=H_c + H_t)$ is the beam height (see Fig. 1). By integrating σ using Eqs. (2) and (1), and after some mathematical manipulations, this force balancing equation finally reduces to

$$\left\{ \frac{1}{R^{n_t + 1}} \hat{k} \frac{n_t - n_c}{n_c (n_t + 1)} \left[\frac{n_c (n_t + 1)}{n_t (n_c + 1)} \right]^{\frac{n_t}{n_t + 1}} \right\} h_c^{\frac{n_t (n_c + 1)}{n_c (n_t + 1)}} + h_c = 1 \quad (3)$$

where $R = A_t/A_c$, $\hat{k} = \dot{K}H/A_c$ and $h_c = H_c/H$ are dimensionless parameters.

Here we choose A_c as normalizing factor for R and \dot{K} presumably because A_c is much easier to measure than A_t . Eq. (3) is a nonlinear algebraic equation of the form $Cx^n + x = 1$ for the unknown h_c quantifying the physical location of the neutral axis. Since both C and n are positive definite, as parameters appeared in Eq. (3) are all positive quantities, it can be proved from the form of this nonlinear algebraic equation that a unique solution for x always exists in the range $0 < x < 1$ beyond which no physical meaning may be assigned to x .

In addition, the requirement that the total summation of moments produced by local tractions be equated to the external moment, M , forms the second governing equation, viz.

$$M = \int_0^{H_c} \sigma Y B dY + \int_0^{H_t} \sigma Y B dY$$

Substitution of Eq. (2) for $\sigma = \sigma(Y)$ and recognition of $h_t + h_c = 1$ result in an equation relating the applied moment to the material's response \hat{k} :

$$m = \hat{k} \left[\frac{1}{n_c} \frac{1}{n_t} - \frac{1}{n_c} \frac{2n_t+1}{n_t} + \frac{n_c}{2n_c+1} h_c \right] \quad (4)$$

where $m = M/(BH^2\sigma_0)$ is the normalized applied moment. The assignment of the reference stress σ_0 is somewhat arbitrary. Since the unit of the applied stress is generally expressed in MPa, it is convenient to set $\sigma_0 = 1$ MPa for simplicity.

Equations (3) and (4) constitute a system of algebraic equations for the two unknowns h_c and \hat{k} , while the remaining parameters such as the applied moment m and the materials parameters A 's and n 's are being treated as given. After examining the structure of these two equations, we arrive at the unfortunate conclusion that analytical solutions in close form cannot be obtained because they are highly nonlinear and coupled in

$\dot{\hat{k}}$. Accordingly, a numerical approach is the practical way to tackle this problem. A computer program was developed which contains the following primary tasks: first the development of a subroutine to solve h_c from Eq. (3) by a Newton-Raphson's iteration scheme. Input to this subroutine are R , n_t , n_c and $\dot{\hat{k}}$, the latter being treated as an independent variable. Note that initially an overshoot outside the range (0,1) for h_c may arise during numerical iterations, stability can then be restored if h_c be reset to its boundary value. Once h_c is successfully solved from this subroutine, it can then be used as input, together with the independent variable $\dot{\hat{k}}$, to Eq. (4) for the computation of m . At the end, a total of three one-dimensional arrays were generated, namely m , $\dot{\hat{k}}$ and h_c . This concludes the computation phase of programming, and the plotting phase follows. The solutions were then displayed in graphic form for $\dot{\hat{k}}$ versus m as well as h_c versus m with any given A's and n's.

2.2 General Solutions

2.2.1 Location of neutral axis, h_c

The solutions for h_c are plotted as a function of m in Fig. 3 for several values of n_t at $n_c = 4.0$, $R = 1000$. Generally speaking for the practical range of $m > 0.5$, as the applied stress increases, the compressive zone keeps shrinking with increasing n_t . Intuitively this must be true since an increase in n_t implies that the material's ability to support tensile stresses is reduced for a fixed creep rate. When $n_t = n_c$, $h_c \approx 0.2$, independent of the applied stress. In fact, h_c can be

expressed analytically in case of equal n . This special case will be discussed later. Another interesting observation that can be extracted from Fig. 3 is that when m is at a value of around one half, h_c is about 0.2 regardless of the value of n_t . As a matter of fact, when examined in a more broader base, we found that when m lies between 0.25 and 0.4 the solutions are quite insensitive to both n_t and n_c suggesting that this range of m should be avoided in a testing program that aims to characterize the materials creep parameters. Fig. 4 presents another solution for h_c for five values of R , fixing values of n_t and n_c at 1 and 5 respectively. As expected, the higher the value of R , the lower the size of compression zone as high R implies that the material's creep resistance in tension is reduced at a given strain rate (or applied moment). When m exceeds 10, however, a major portion of the beam is in compression for R values up to 1000. Conversely, setting $n_t = 5$ and $n_c = 1$ demonstrated a reverse trend, as shown in Fig. 5 for the same five values of R . Again, cases of higher R result in smaller compression zone as expected.

2.2.2 Curvature rate of a beam element, $\dot{\hat{k}}$

The materials response in the form of curvature rate $\dot{\hat{k}}$ under creep bending for a given applied moment m is plotted in Fig. 6 on a log-log scale for five values of n_t and fixing $n_c = 4$ and $R = 1000$. Two important observations can be made here: (1) the curves appear linear with, of course, always positive slopes when n_t 's are in the neighborhood of n_c but when the gap between the values of n_t and n_c widens, the curves become nonlinear and concave upward; (2) a "blind point" in the vicinity of $m = 1/2$ is also observed, similar to the solutions of h_c . Fig. 7

demonstrates the solutions of \hat{k} upon variation of R under fixed values of $n_t = 1$ and $n_c = 5$. Again, owing to big differences between the values of n_t and n_c , concave upward curves are obtained. Another interesting feature noteworthy to state is the solutions converge into one single straight curve as the applied moment exceeds 15. This means that applying a load in excess of $m = 15$, would generate a straight line in \hat{k} vs m plot, regardless of the values of R and therefore is not particularly useful. Lower loads (much less than $m = 15$) are thus recommended. If, on the other hand, $n_t = 5 \gg n_c = 1$ then the solutions are well-behaved in the practical range of the applied load ($.01 \leq m \leq 100$) as indicated in Fig. 8, although most of the solutions appear to be linear.

2.2.3 Outer fibre stresses, σ_c and σ_t

As can be seen from the preceding section, during steady state creep the neutral axis is displaced from the centroid and the stress distributions are highly non-linear. As a result, it is to be expected that the outer fibre stresses, both at the tensile side as well as at the compression side must in general differ from the initial elastic stress levels. In terms of the applied bending moment M, the outer fibre elastic stresses both in tension and in compression have a value $\sigma_e = 6M/(BH^2)$ from classical simple beam theory, and in terms of dimensionless quantities, there results $\hat{\sigma}_e = 6 m$, where $\hat{\sigma}_e = \sigma_e/\sigma_0$ is the normalized outer fibre elastic stress.

The steady-state compressive creep stress at the outer surface of the beam is

$$\sigma_c = \sigma_o (k h_c)^{1/n_c}$$

as evidenced from Eq. (2). Normalizing against σ_e we have

$$\sigma_c / \sigma_e = \frac{1}{6m} (k h_c)^{1/n_c} \quad (5)$$

Similarly the creep stress at the tensile edge, also normalized by σ_e is

$$\frac{\sigma_t}{\sigma_e} = \frac{1}{6m} [k (1-h_c)/R]^{1/n_t} \quad (6)$$

Examination of these two equations indicates that the outer fibre creep stresses, unlike their elastic counterpart, are not only a function of applied moment, but also dependent on the neutral axis location and the intrinsic power-law creep parameters. The maximum compressive stresses for several n_t are plotted in Fig. 9, according to Eq. (5) for typical values of $n_c = 4$ and $R = 1000$. When $m < 0.35$ corresponding to an elastic stress of about 2 MPa, higher values of n_t yield lower compressive stresses; the reverse situation occurs if the applied stress exceeds 2 MPa. On the other hand, the maximum tensile stresses at the outer fibre, as plotted in Fig. 10 from Eq. (6), show a unique feature, namely for a fixed applied load, in the practical range (1 - 600 MPa) low values of n_t yield higher tensile creep stresses. Note that in both cases, as shown in

Figs. 9 and 10, in the case of $n_c = n_t$, the outer fibre stresses are independent of the applied moment and as will be shown later in Sec. 2.3 they can be expressed in closed forms.

2.2.4 Load-point displacement rate, $\dot{\Delta}_p$

As demonstrated in the preceding sections, $\dot{\kappa}$ is a proper parameter to measure the response of creep for a bend bar under the constant applied moments. Unfortunately, the curvature time-rate of a beam at a fixed location is difficult to measure in the laboratory and it is a general practice to measure instead the load-point displacements continuously as a function of time. Hence, it is desirable to present solutions in terms of $\dot{\Delta}_p$.

For a given material with a well defined $\dot{\kappa}$ vs m relationship the load-point displacement rate $\dot{\Delta}_p$ incurred from a four-point bend beam can be solved numerically by integration of $\dot{\kappa}$ along the beam length x with linear moment distribution in the outer span and a constant maximum moment in the inner span. Here, it is assumed that shear effects on the beam deflection y are negligible and the slopes of the deformed beam shape are small ($dy/dx \ll 1$). The differential equation that needs to be solved is then $d^2\dot{y}/dx^2 = \dot{\kappa}(x) = f(m)$ with $\dot{\kappa} = f(m)$ given in Sec. 2.2.2. Setting the origin of the coordinate system at the mid span of the deformed beam, the proper boundary conditions are $y(0) = 0$ and $y'(0) = 0$ due to symmetry. After the deformed shapes $\dot{y} = \dot{y}(x)$ are solved, the load-point displacement rate is given by $\dot{\Delta}_p = \dot{y}(L/2) - \dot{y}(\ell/2)$ where L and ℓ are the lengths of major and minor spans respectively. Typical solutions are plotted in Fig.

11 for nondimensional load-point displacement rate, defined as $\dot{\Delta}_p/HA_c$ as a function of the applied moment m for several values of n_t with $n_c = 4$, $R = 1000$, $L = 4\ell$ and $H/\ell = 1/2$. Similarities between Fig. 6 and 11 are observed. Whenever $n_c = n_t = N$, the solution can be described by a linear curve owing to the fact that the relationship between \dot{K}_p and $\dot{\Delta}_p$ is linear and has a form

$$\dot{K}_p = \frac{4(N+2)}{(L-\ell)[L+(N+1)\ell]} \dot{\Delta}_p$$

2.3 The special cases

Having obtained the general solutions in the previous section, it is easy to arrive at the results for the special cases as considered by Hollenberg et al. [4] and Talty and Dirks [10].

2.3.1 The case $n_t = n_c = N$; $R \neq 1$

This is the case considered by Talty and Dirks [10] and Cohrt et al. [12]. For this case, Eq. 3 describing the location of neutral axis takes the following simple form

$$h_c = \frac{1}{1 + R^{1/(N+1)}} \quad (7)$$

independent of the applied moment m . This is in agreement with the work of Cohrt et al. [12] (See Eq. 3 of Ref. 12 in which our R is equivalent to their S^n). In addition, it can be shown from Eq. 4 that the moment vs curvature rate is linear when plotted on logarithmic scales, and therefore can be described by

$$\dot{k} = C m^N \quad (8)$$

where C is the intercept at $m = 1$ and is only a function of h_c , R and N:

$$C = \left[\frac{(2N + 1)/N}{h_c \frac{2N+1}{N} + (1-h_c) \frac{2N+1}{N}} R^{1/N} \right]^N \quad (9)$$

Fig. 12 presents the solutions of h_c for several N, based on Eq. (7) as a function of C defined in Eq. (9). Fig. 13 demonstrates the solutions for

R. If $n_c = n_t = N$, the bend test data in terms of \dot{k} vs m ought to be fitted by a linear curve on logarithmic axis. A_c is automatically obtainable from \dot{k} and \dot{K} (see Fig. 1 and definition of \dot{K}). C as well as N can then be extracted from this curve. Figs. 12 and 13 can then be used to obtain h_c and R (hence A_t) and the complete creep parameters are determined.

2.3.2 The case of uniform property ($n_t = n_c = N$; $R = 1$)

This case has already been considered by Hollenberg et al. [4]. The neutral axis in this case always coincides with the centroid (i.e. $h_c = 1/2$) as can be shown from Eq. 7 when $R = 1$ is substituted.

Constitutive equation 8 describing the relations between \dot{k} and m is of course still valid but the intercept C now takes the simple form:

$$C(N) = 2 \left(\frac{2N+1}{N/2} \right)^N \quad (10)$$

Fig. 14 is a plot of N against C from Eq. (10). This can be used as a first step to check whether the material has uniform properties in creep by checking the observed value of C to see if it agrees with the predicted value of C given by this plot.

2.4 Application

As an example of demonstrating the applicability of the present analysis, three loads of different magnitude were applied to debased alumina (commercially known as AD-86¹/₁ from Coors Corporation) beams at 1100°C in a four-point bend configuration with major and minor spans set at 40 and 10 mm respectively. Load-point displacements are continuously monitored as a function of time. Apparent steady-state was observed in all cases within 40 hour duration. Table I lists the pertinent data of measurements. After data were taken, the first step is to plot $\dot{\Delta}_p$ versus m on logarithmic scales. If the resulting curves are linear, the solutions presented in Sec. 2.3 can be used to check whether special cases apply. Since plotting of data in Table I indicated non-linear behavior (suggesting $n_t \neq n_c$), the special cases discussed in Sec. 2.3 must be ruled out. Solutions of different R and n were produced in order to fit the data points. It was finally found that a special curve as shown in Fig. 15 with the following constants $n_c = 4$, $n_t = 1/2$, $R = 50,000$ fits the

¹/ Certain commercial equipment, instrument or materials are identified in this paper in order to adequately specify the experimental procedure. Such identification does not imply recommendation or endorsement by the NBS, nor does it imply that the materials identified are necessarily the best available for the purpose.

data well. A_c was determined from the solution to be $0.85 \times 10^{-13} \text{ s}^{-1}$. Thus the steady-state tension creep behavior of this refractory material can be described by

$$\dot{\epsilon}_{st} = 4.25 \times 10^{-9} \sigma^{1/2}$$

and the compression creep, on the other hand, by

$$\dot{\epsilon}_{sc} = 0.885 \times 10^{-13} \sigma^4$$

where $\dot{\epsilon}$ and σ have the units of s^{-1} and MPa respectively.

The predictions strongly suggest a profound difference of creep behavior between tension and compression. Uniaxial tension tests were also performed which yield the same order of magnitude as predicted by the current analysis. Additional tests in simple tension as well as in compression are being performed in order to verify the predictions. Detailed microstructures of these post crept beam specimens are also being investigated in order to understand the rheology leading to the resulting power-law stress exponents. One dominating factor obtained from the preliminary studies is the observation of compositional changes due to devitrification, resulting in drastic variation of viscosity in the grain boundary liquid phases [15-16]. This strong stress-dependent viscosity coupled with local recrystallization in the compression zone and dilatancy and/or cavitation in the tension region may be responsible for the unequal stress exponents.

In contrast, the conventional method assumes $R = 1$ and $n_t = n_c = N$ so that the outer fibre creep rate can be computed from the load-point displacement rate data by the following equation

$$\dot{\epsilon}_{ss} = \frac{2(N+2)H\dot{\Delta}_p}{(L-l)[L+(N+1)l]}$$

and the outer fiber stresses by

$$\sigma = \sigma_e \left(\frac{2N+1}{3N} \right)$$

Table II lists the resulting outer fiber creep rates and stresses computed from the same set of load point displacement data tabulated in Table I. A plot of $\dot{\epsilon}_{ss}$ versus σ_e on logarithmic scales by least squares method as shown in Fig. 15 leads to a prediction of $A = 1.71 \times 10^{-11} \text{ s}^{-1}$ and $N = 1.86$. Hence we see there are substantial differences in the prediction of power-law creep parameters between the present analysis and the conventional method. Notice that $A_t < A < A_c$ and $n_t < N < n_c$ implying that the conventional techniques, by imposing uniform properties, effectively generate an average response in bending creep.

3. Discussion

We have presented a viable technique by which individual tension and compression creep behaviors, being equal or not, can be predicted directly from bend test data. Several main features in the analysis are noteworthy: (1) the neutral axis of the beam cross-section is, in general not located at the centroid, the location is not only a function of the materials constants but also of the applied loads. This is generally indicated by observations of significant densities of cavities developed over 50 percent of the beam cross section, suggesting the neutral axis has

migrated towards the compressive side. (2) If a plot of data on $\dot{\epsilon}$ vs m shows strong non-linearity which is concave upward, there will be a big difference between n_c and n_t . (3) There exists an applied load for all materials, in the neighborhood of 1 ~ 2 MPa of initial outer fibre elastic stress, under which the material response in $\dot{\epsilon}$ or $\dot{\Delta}_p$ will be insensitive to n 's suggesting that this load level is not useful in the test program.

(4) If $\dot{\epsilon}$ vs. m data demonstrates a linear response on logarithmic axes, then the results given in Sec. 2.3 can be first used to ascertain whether the material poses uniform creep properties. Otherwise, the general solution scheme as detailed in Sec. 2.1 has to be adopted since a linear curve within a short range of m does not necessarily mean that $n_t = n_c$ as evidenced from Fig. 7. An example was given in Sec. 2 to show how to apply the current analysis to a realistic case.

However, the analysis does have some restrictions and limitations built-in which ought to be borne in mind. First, the constitutive law is assumed to take a power-law equation form with the distinction being made through the variations in n and A . Microscopic observations including SEM and STEM have showed that in a general ceramic system, cracks and cavities are developed in different patterns both in terms of density and orientations inside the tensile and compressive zones of a crept bend specimen. Hence, cracking and cavitation play an important role in the contribution to creep resulting in distinct behaviors. Secondly, no deformation mechanism changes are assumed to take place under uniaxial loading so that a single power-law equation completely characterizes the creep behavior. Consequently, the current analysis is not applicable to materials exhibiting bi-linear law, although in principle, a numerical

scheme may be developed to handle this case. Finally the problem of creep fracture is not addressed in this paper. As a result, the solutions presented here are assumed to be valid irrespective of how high the loads are applied. Realistically, however, as the loads become higher and higher, the solutions will always be termed invalid somewhere by premature failure due to void growth and flaw linkage. The prediction of rupture time as a function of applied stress is thus an important area which warrants further studies.

Rosenfield et al. [8] recently presented a similar time-independent analysis on a beam with three different tensile laws. By fixing the compression behavior as linearly elastic, they found an interesting result that at $1/5$ of the beam depth from the tension edge, the stress there is fairly fixed regardless of the form of the tensile deformation law. However, with the removal of the assumption of linear behavior in compression, the results given by the present analysis did not show this feature. Accordingly, we must conclude that their results possess a strong limitation induced by the imposed linear elastic behavior in compression.

4. Summary and Recommendations

In lieu of summary of the analysis presented in the paper, the following recommendations are offered to experimenters who intend to use bend tests for characterizing the materials creep behavior:

- (1) The range of the applied loads should be as wide as possible; at least two orders of magnitude in loads (e.g. 5 - 600 MPa) are recommended.

(2) In case that higher moments cannot be achieved owing to premature fracture a supplemental test program either in tension or in compression should be performed for the purpose of reducing computer work, thus improving the accuracy of the results.

(3) Direct measurement, of uniform curvature rate in the inner span are preferred to load-point displacements measurements as the latter induce complications such as shearing effects, although the former may be more difficult to do.

Acknowledgments

Financial support by AR&TD Fossil Energy Materials program of the U.S. Department of Energy under interagency agreement DE-A105-800R20679 and by the U.S. Air Force Office of Scientific Research under the agreement AFOSR-ISSA-84-00013 with NBS are hereby acknowledged. The author is grateful to Professor Karl Jakus of the University of Massachusetts, Amherst, MA for carrying out the bending experiment on glass-bonded alumina, and to Drs. Richard J. Fields and Sheldon M. Wiederhorn of NBS for critically reviewing the manuscript.

References

1. S.U. Din and P.S. Nicholson, J. Mater. Sci. 10 (1975) 1375.
2. S.U. Din and P.S. Nicholson, J. Am. Ceram. Soc. 58 (1975) 500.
3. W.R. Cannon and T.G. Langdon, J. Mater. Sci. 18 (1983) 1.
4. G.W. Hollenberg, G.R. Terwilliger and R.S. Gordon, J. Am. Ceram. Soc. 54 (1971) 196.
5. M.S. Seltzer, Bul. Am. Ceram. Soc. 56 (1977) 418.
6. R. Morrell and K.H.G. Ashbee, J. Mater. Sci. 8 (1973) 1253.
7. D. Krajcinovic, J. Appl. Mech. 46 (1979) 592.

8. A.R. Rosenfield, D.K. Shetty and W.H. Duckworth, to appear in J. Mater. Sci.
9. I. Finnie, J. Am. Ceram. Soc. 49 (1966) 218.
10. P.K. Talty and R.A. Dirks, J. Mater. Sci. 13 (1978) 580.
11. T. Fett and D. Munz, *ibid.* 19 (1984) 1791.
12. H. Cohrt, G. Grathwohl and F. Thgummler, Res. Mechanica, 10 (1984) 55.
13. R.M. Arons and J.K. Tien, J. Mater Sci. 15 (1980) 2046.
14. G.H. MacCullough, Trans. ASME (1933) 55.
15. S.M. Wiederhorn, B.J. Hockey, R.F. Krause and K. Jakus, submitted to J. Mater. Sci.
16. W.D. Kingery, H.K. Bowen and D.R. Uhlmann, "Introduction to Ceramics", John Wiley & Sons, Inc. (1976) p. 757.

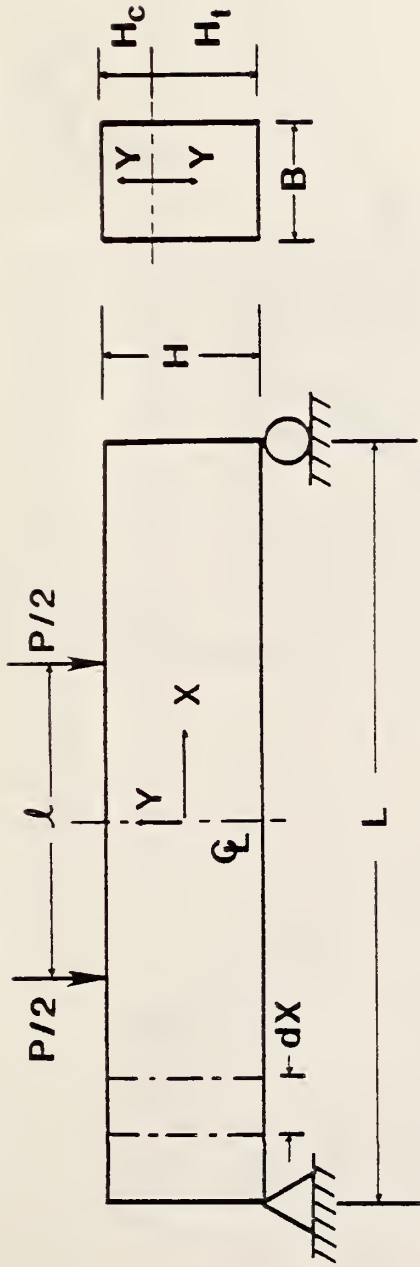
Table I. Calculations of normalized load-point displacement rates from 4-point bend data of glass alumina tested at 1100°C. Power-law creep parameters were then obtained based on the present analysis.

Specimen No.	Beam Height H (mm)	σ_e (MPa)	m	$\dot{\Delta}_p$ ($\times 10^{10}$ m/s)	$\dot{\Delta}_p/H$ ($\times 10^7$ s $^{-1}$)	$\dot{\Delta}_p/HA_c$ ($\times 10^{-6}$)
1	2.785	20	3.333	5.185	1.862	2.191
2	2.785	20	3.333	4.719	2.694	1.993
3	2.770	30	5.000	6.311	2.278	2.680
4	2.770	30	5.000	6.656	2.403	2.827
5	2.770	40	6.666	11.50	4.152	4.885
6	2.770	40	6.666	11.57	4.177	4.914

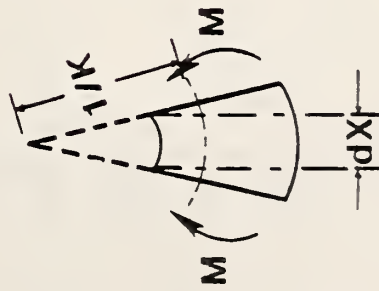
Table II. Computation of strain rates for the same set of data listed in Table I. Different power law creep parameters were then predicted based on conventional method.

Specimen No.	Beam Height H (mm)	Outer Fibre Elastic Stresses σ_e (MPa)	Outer Fibre Creep Stresses σ (MPa)	$\dot{\Delta}_p$ ($\times 10^{10}$ m/s)	Creep Rate $\dot{\epsilon}_{ss}$ ($\times 10^9$ s $^{-1}$)
1	2.785	20	16.93	5.185	5.417
2	2.785	20	16.93	4.719	4.930
3	2.770	30	25.40	6.311	6.557
4	2.770	30	25.40	6.656	6.916
5	2.770	40	33.87	11.50	11.951
6	2.770	40	33.87	11.57	12.020

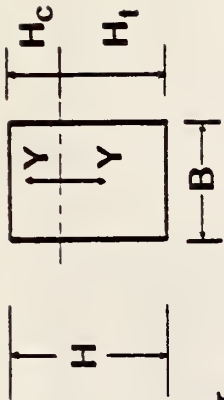
Note: $\sigma = \left(\frac{2N+1}{3N}\right)\sigma_e, \dot{\epsilon}_{ss} = \frac{2(N+2)H\dot{\Delta}_p}{(L-l)[L+(N+1)l]}$; $N = 1.86, L = 40$ mm, $l = 10$ mm .



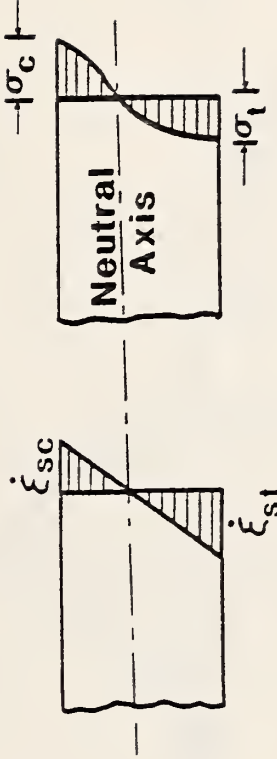
(a)



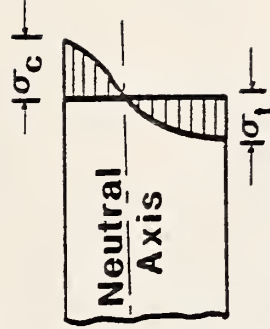
(c)



(b)



(d)



(e)

Fig. 1. Schematic sketches of a four-point bend beam. (a) loading configuration (b) representative cross-section (c) typical element of deformed shape (d) strain-rate distribution and (e) stress distribution.

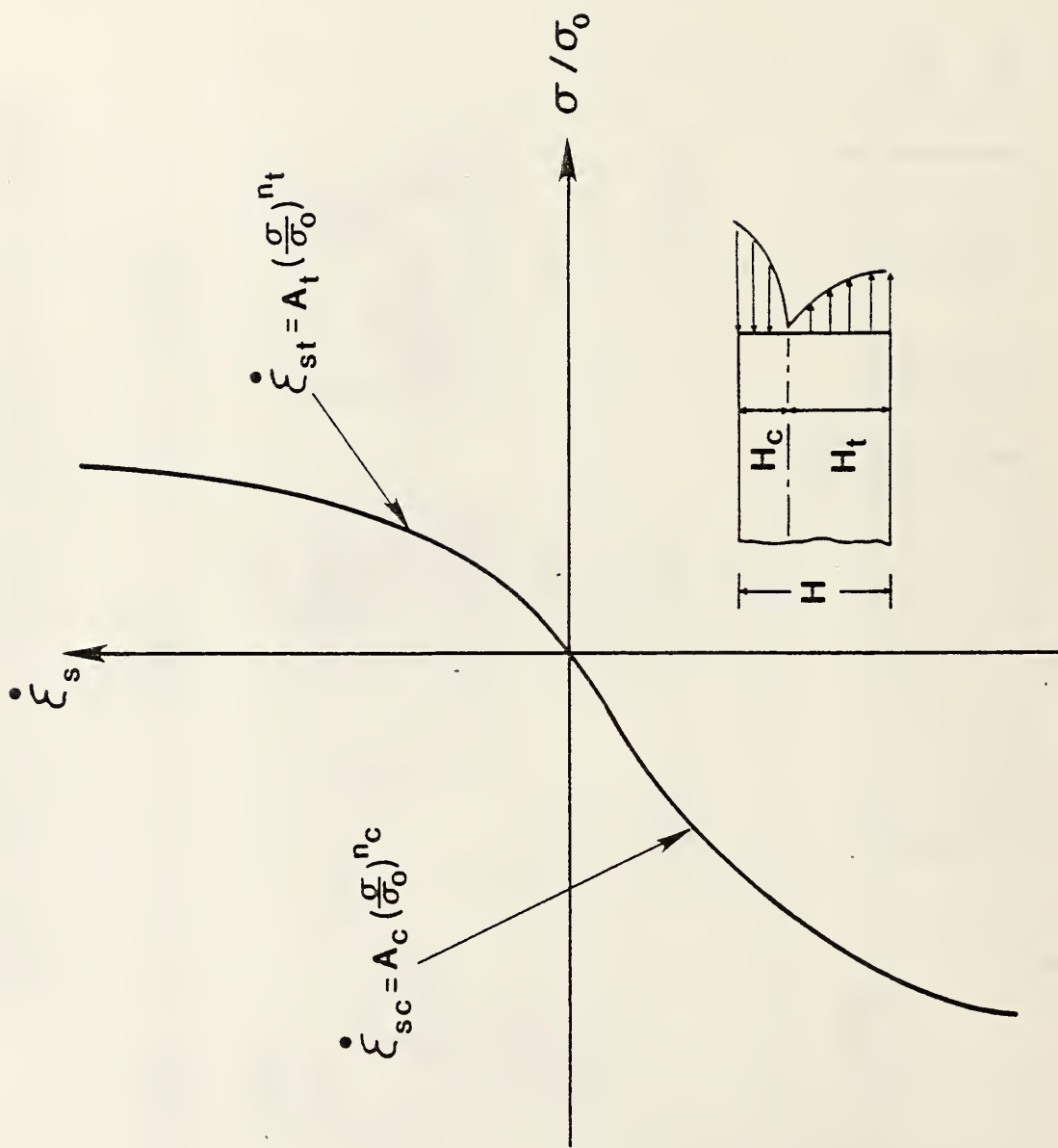


Fig. 2. Schematic of power-law constitutive equations in creep showing distinct behaviors between tension and compression.

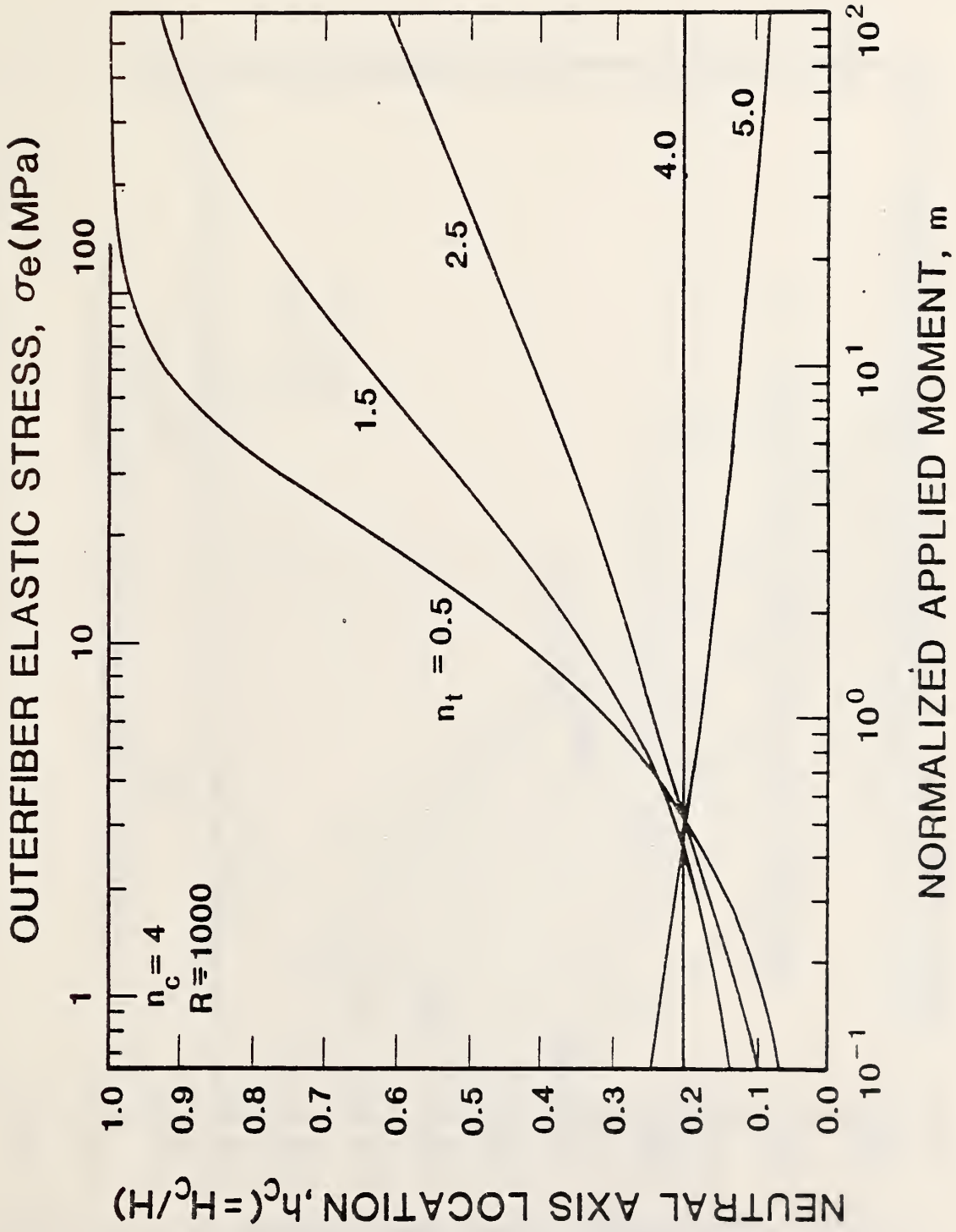


Fig. 3. Solutions for normalized compressive size h_c as a function of the applied bending moment, m , at $n_c = 4$, $R = 1000$ and $n_t = 0.5, 1.5, 2.5, 4.0$ and 5.0 respectively.

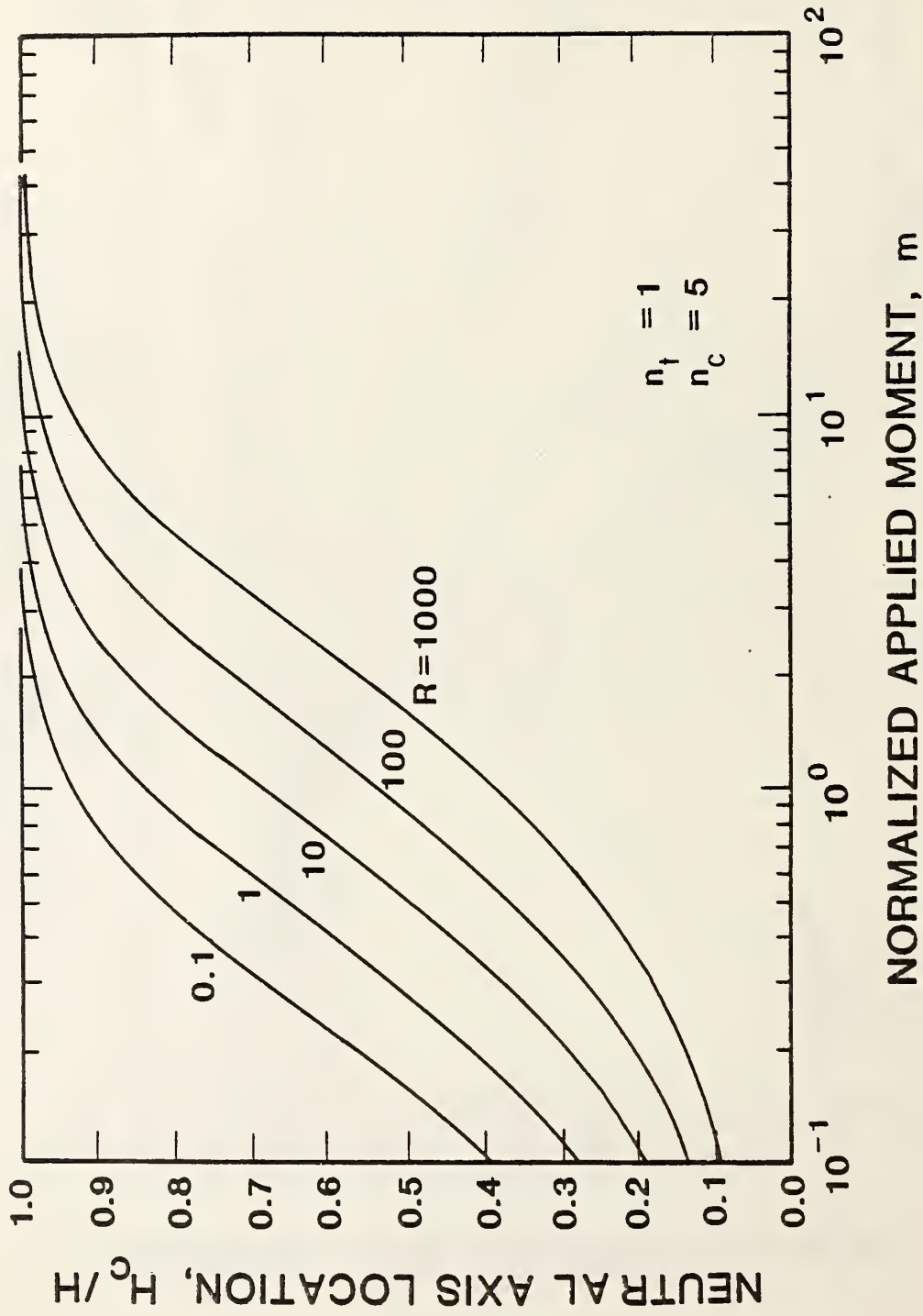


Fig. 4. Plots of neutral axis location versus the applied moment for $n_t = 1$, $n_c = 5$ and $R = 0.1, 1, 10, 100$ and 1000 respectively.

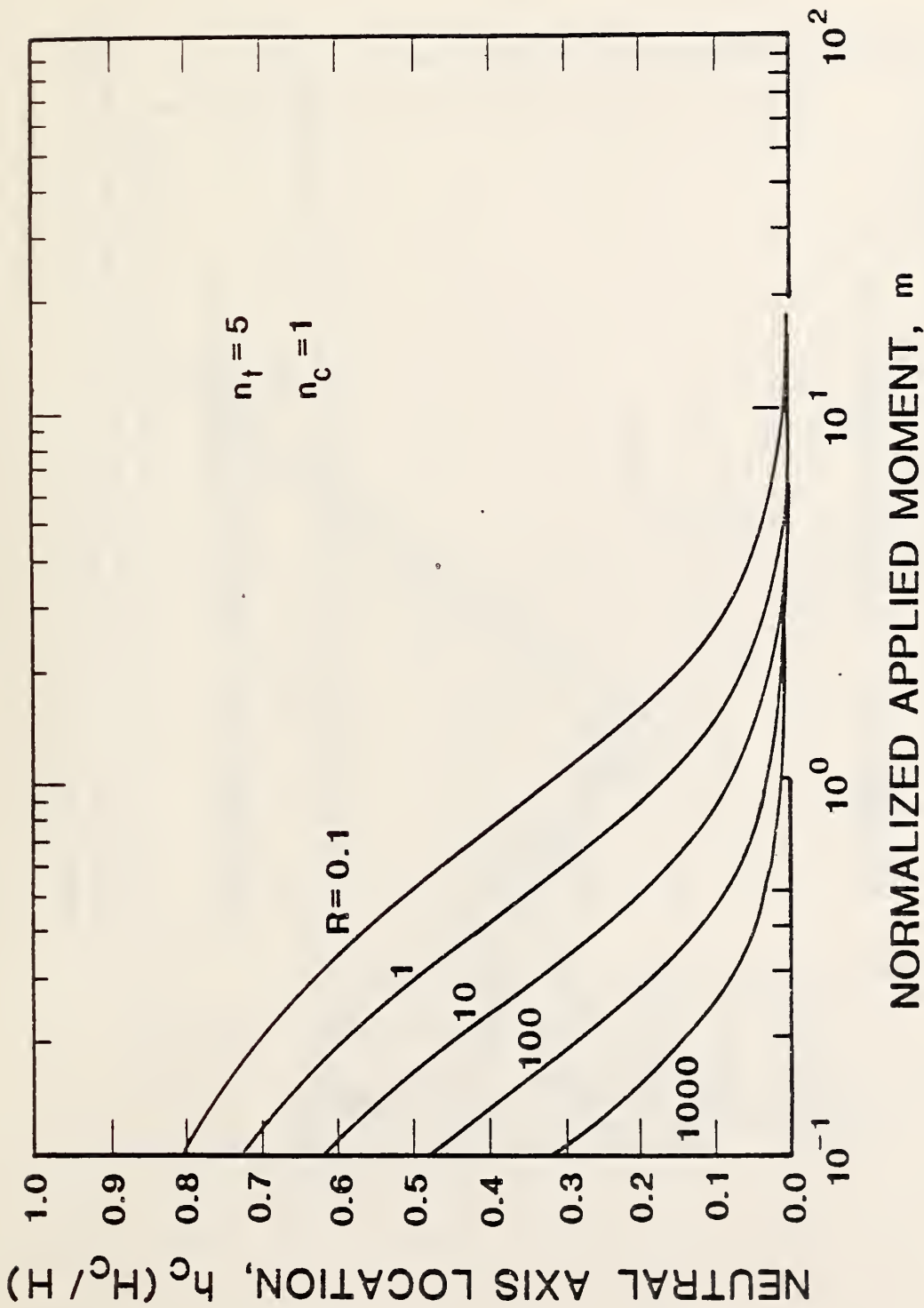


Fig. 5. Compressive zone size solutions as a function of the applied moment at $n_t = 5$, $n_c = 1$ and $R = 0.1, 1, 10, 100$ and 1000 respectively.

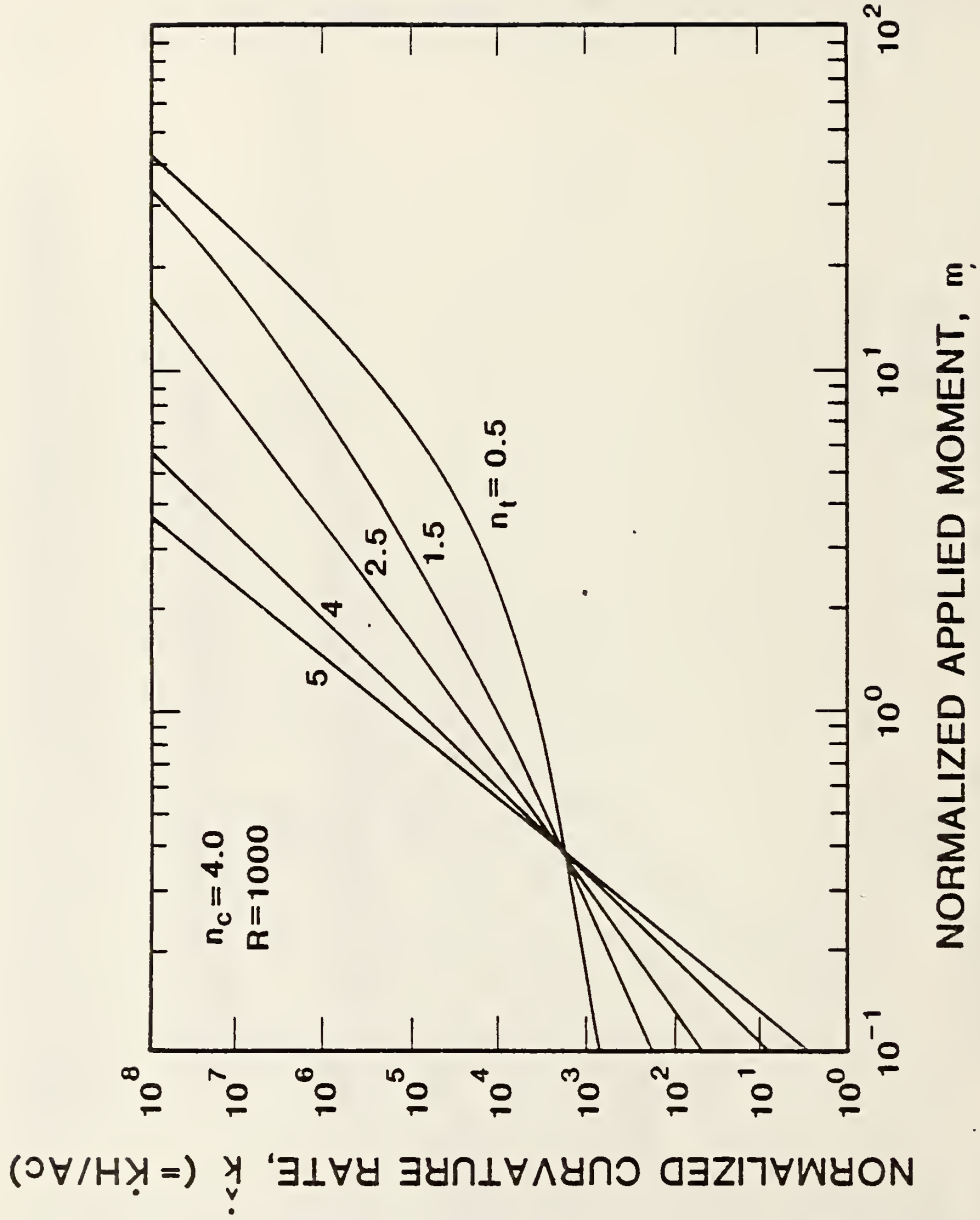


Fig. 6. Solutions of normalized curvature rate as a function of applied moment for $n_c = 4$, $R = 1000$ and $n_t = 0.5, 1.5, 2.5, 4$ and 5 respectively.

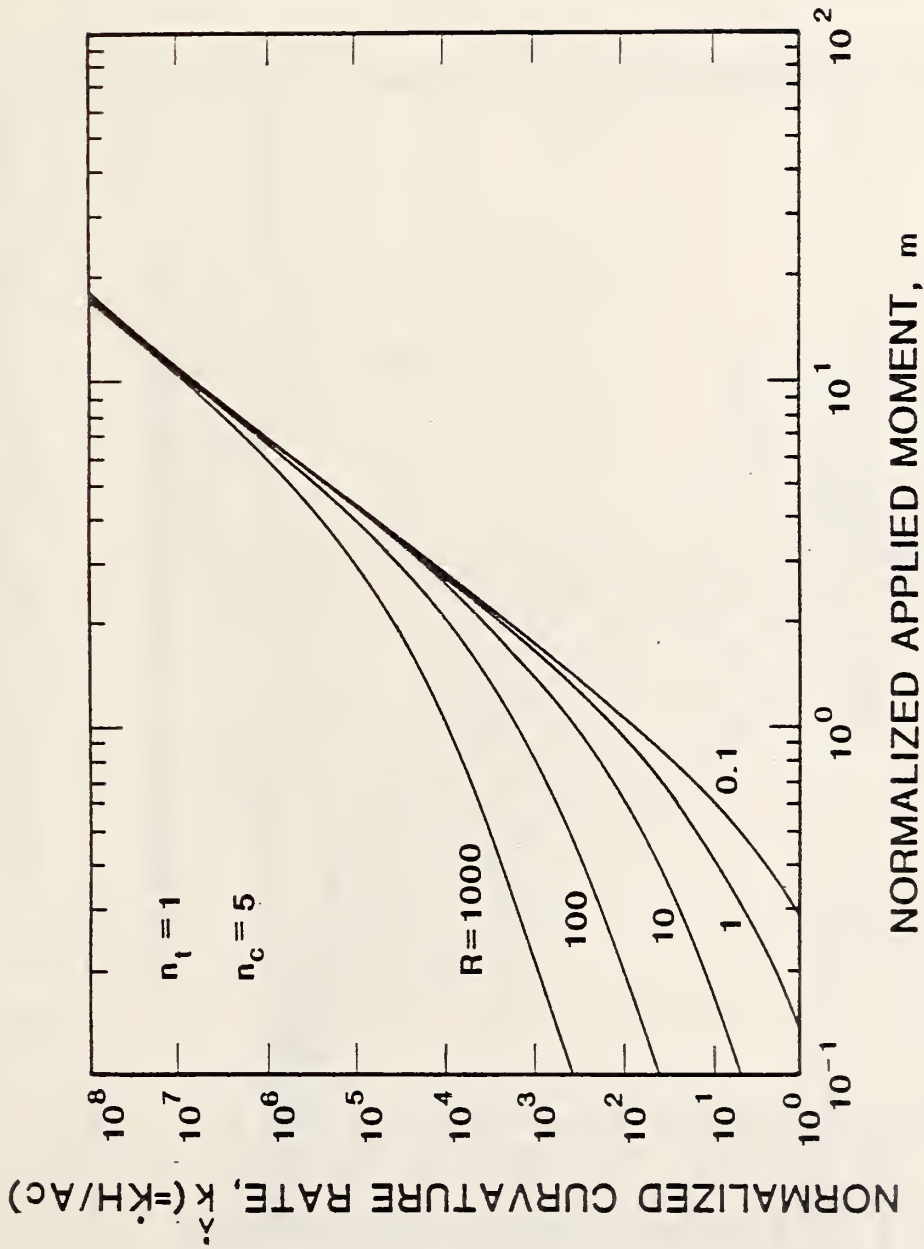


Fig. 7. Typical plots of \dot{k} vs m for $n_t = 1$, $n_c = 5$ and $R = 0.1, 1.0, 10, 100$ and 1000 respectively.

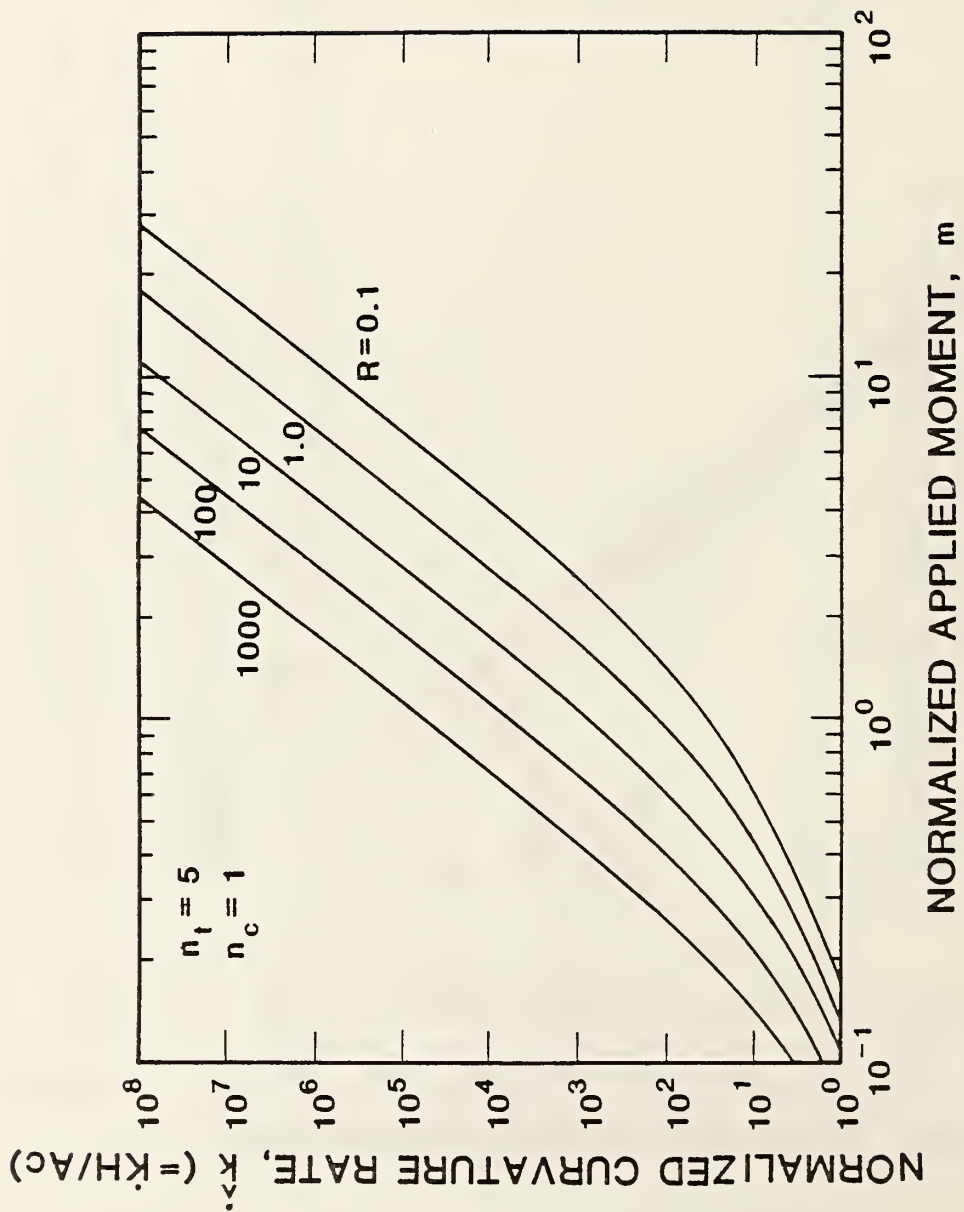


Fig. 8. Similar plot as Fig. 7 except $n_t = 5$ and $n_c = 1$.

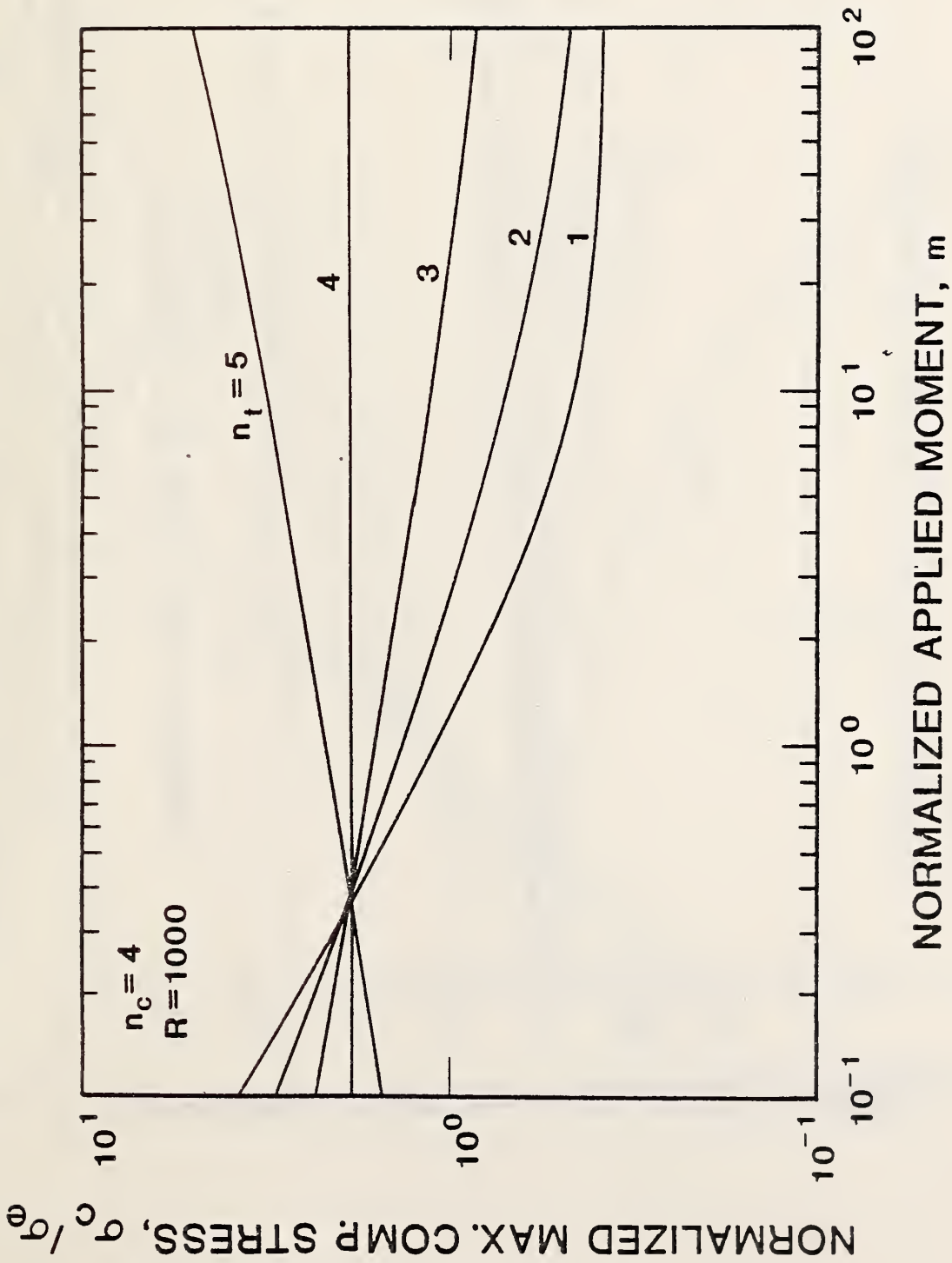


Fig. 9. Plots of outer fibre compressive creep stress normalized against elastic stress versus applied moment for $n_c = 4$, $R = 1000$ and $n_t = 1, 2, 3, 4$ and 5 respectively.

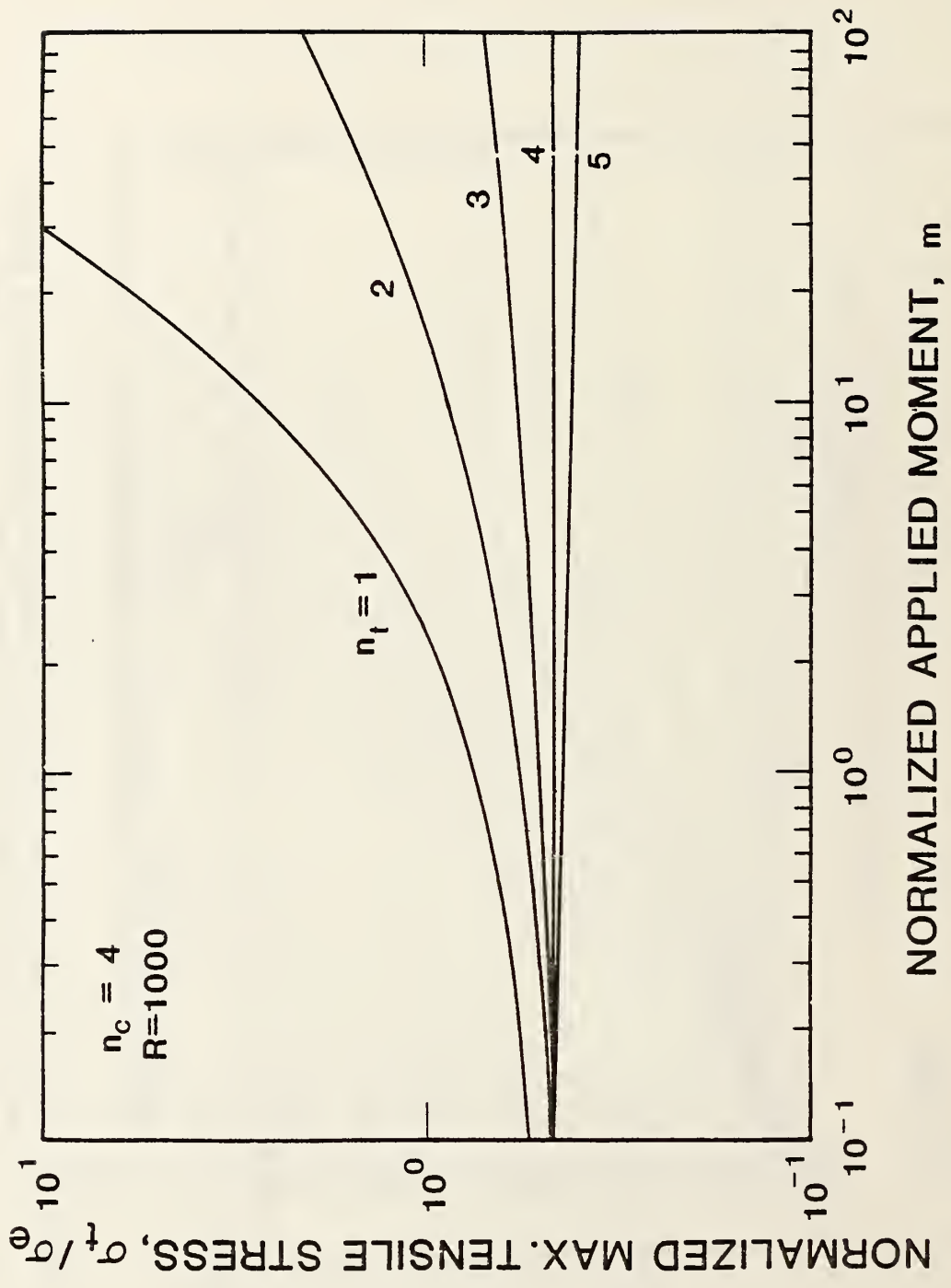


Fig. 10. Numerical solutions for normalized outer fibre tensile stress, (σ_t/σ_e) as a function of m . The materials constants are the same as in Fig. 9.

INITIAL OUTERFIBER ELASTIC STRESS, σ_e (MPa)

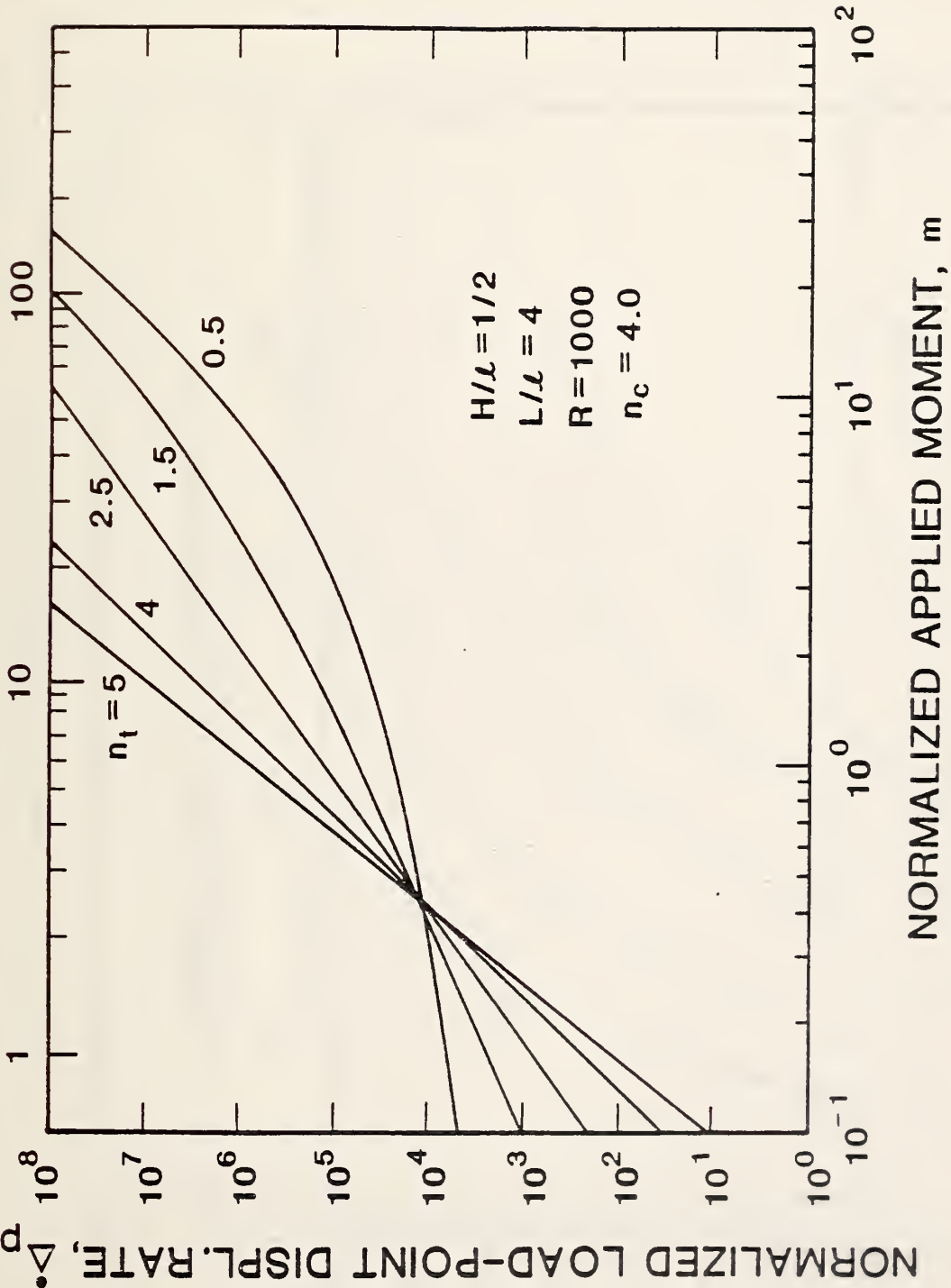


Fig. 11. Plots of load-point displacement rate versus m for several values of n_t at $n_c = 4$ and $R = 1000$.

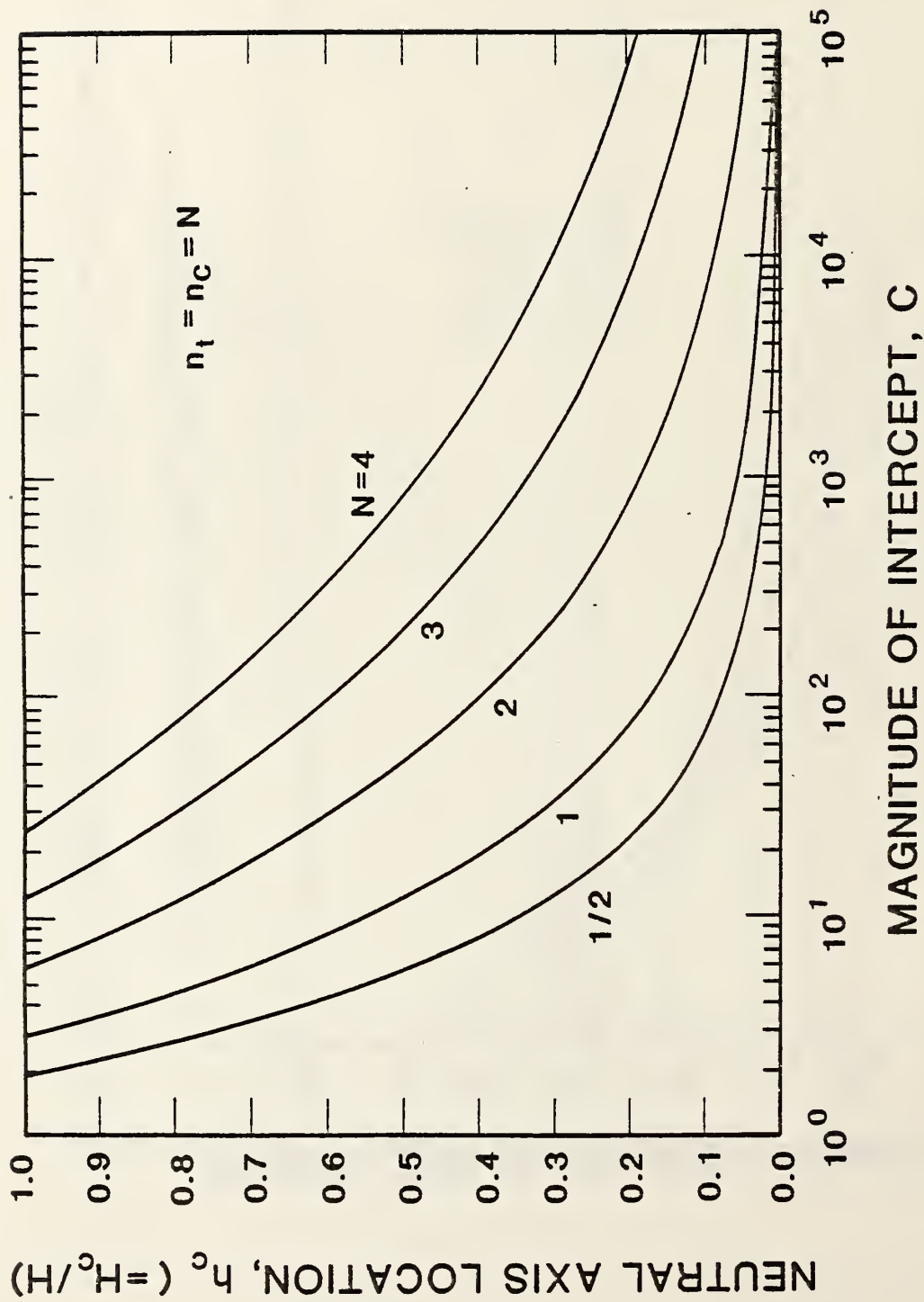


Fig. 12. Plots of h_c vs C , C being the intercept of the linear curves on \dot{k} vs m at $m = 1$, thus is a measurable parameter.

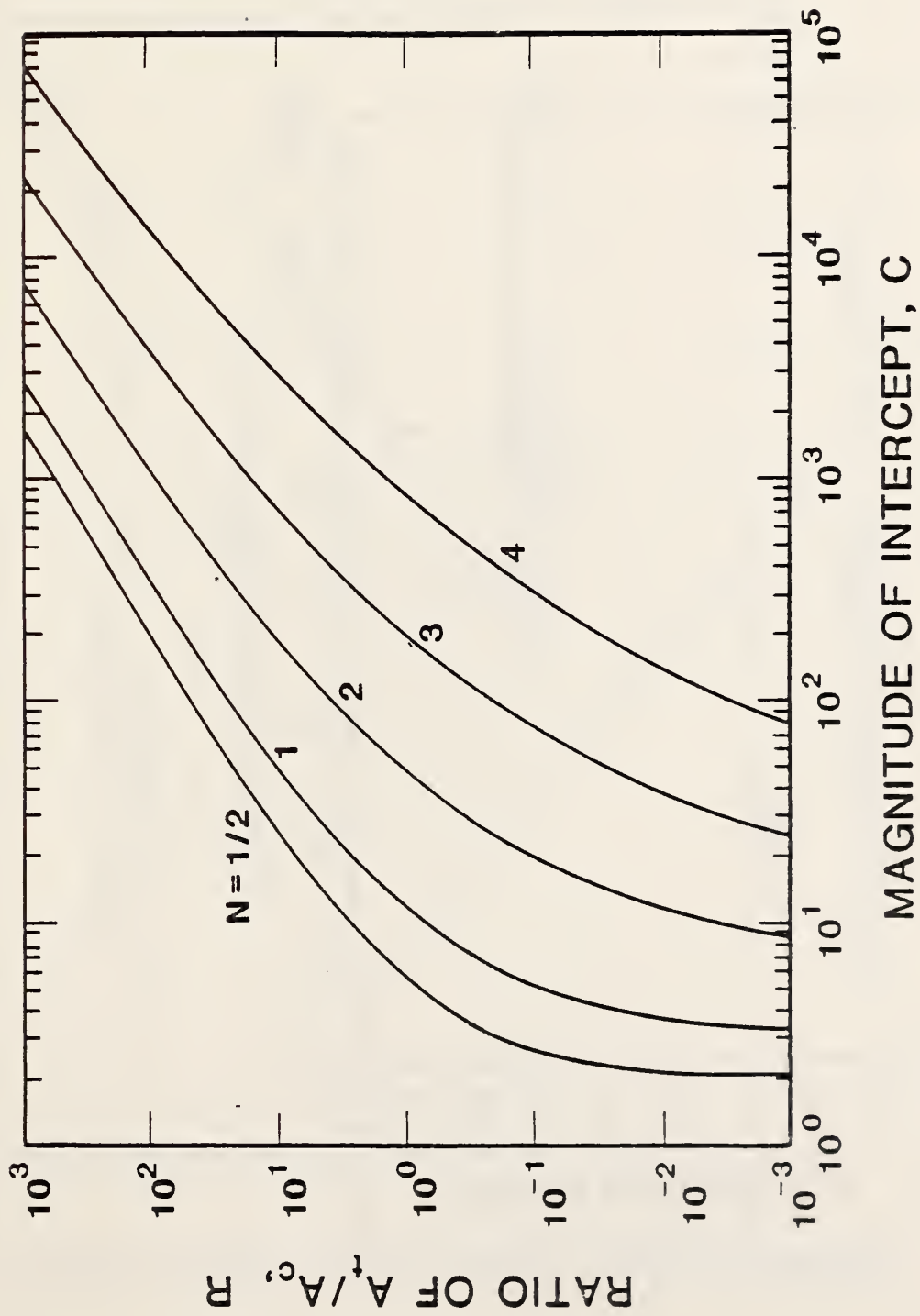


Fig. 13. Plots of R vs C for the same fixed value of N .

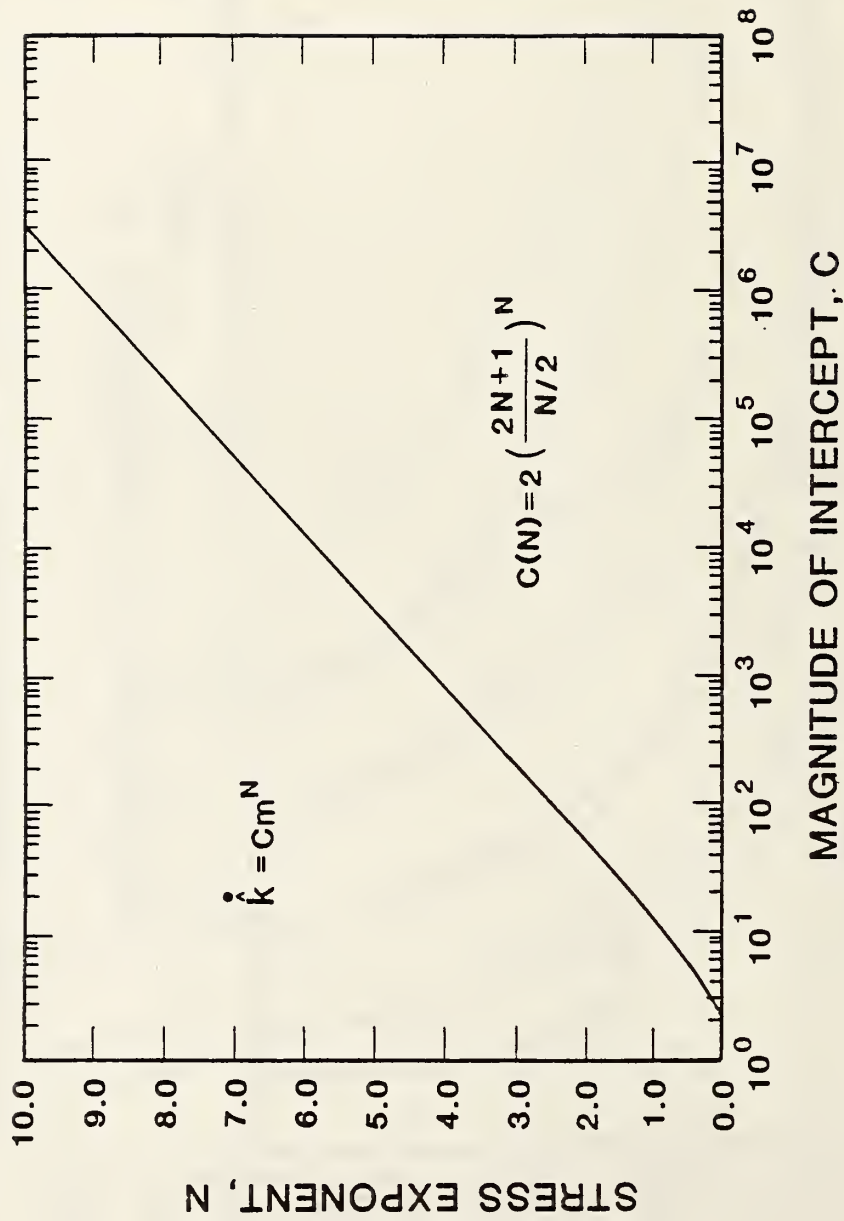


Fig. 14. Plots of N vs C when $R = 1$ and $n_t = n_c = N$.

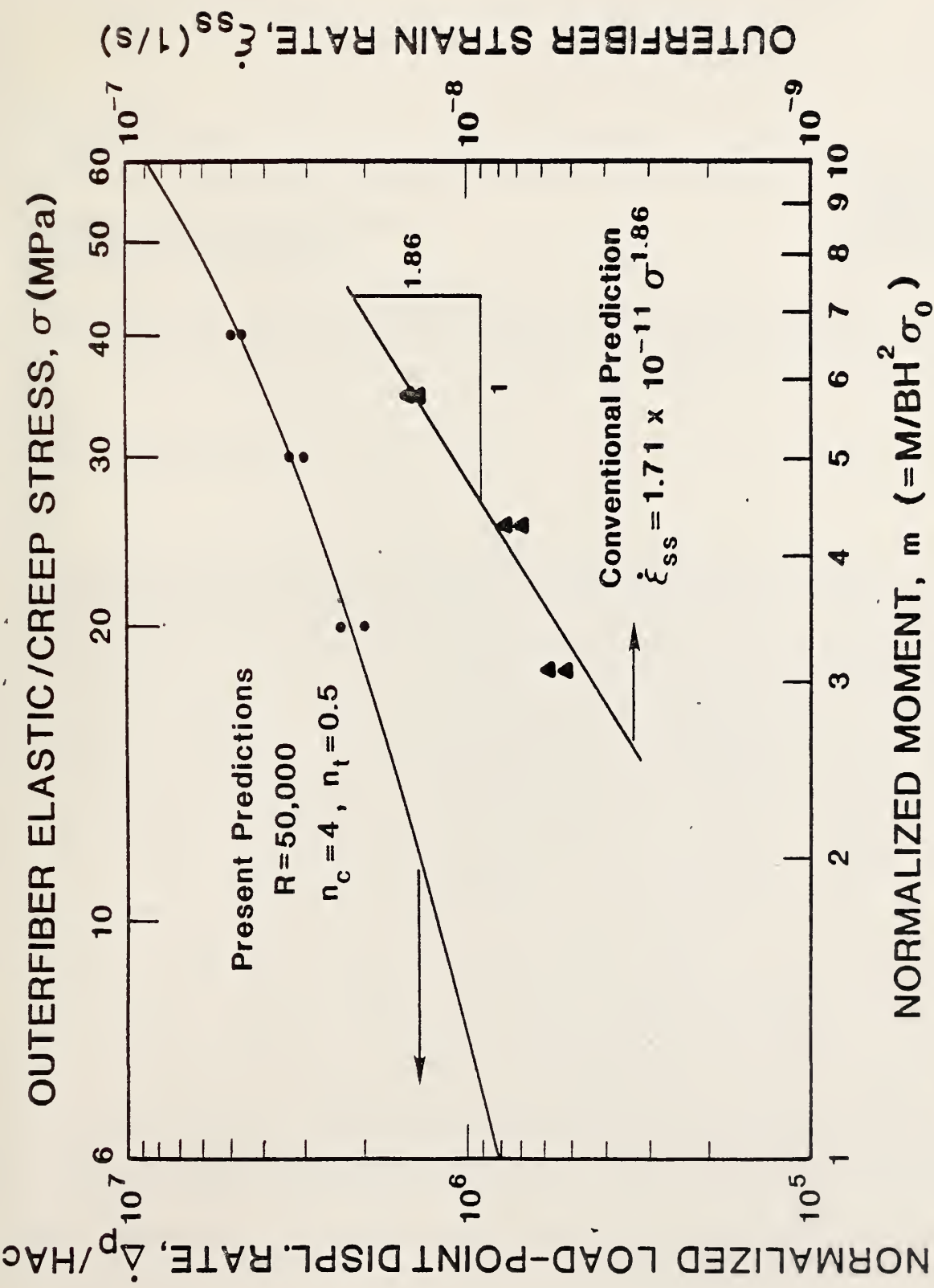


Fig. 15. Plot of four-point bend test data on glass alumina crept at 1100°C in the space of $\log(\dot{\Delta}_p/HA_C)$ versus $\log m$ indicating a good match at a solution for $R = 50,000$, $n_c = 4$ and $n_t = 1/2$. The power-law creep parameters are then predicted as $A_c = 0.85 \times 10^{-13} s^{-1}$, $n_c = 4$; $A_t = 4.25 \times 10^{-9} s^{-1}$, $n_t = 1/2$. For comparison purposes, a linear plot based on the conventional method is also given.

U.S. DEPT. OF COMM. BIBLIOGRAPHIC DATA SHEET (See instructions)	1. PUBLICATION OR REPORT NO. NBSIR 85-2997	2. Performing Organ. Report No.	3. Publication Date February 1985
4. TITLE AND SUBTITLE Estimation of Power-law Creep Parameters from Bend Test Data			
5. AUTHOR(S) Tze-jeer Chuang			
6. PERFORMING ORGANIZATION (If joint or other than NBS, see instructions) NATIONAL BUREAU OF STANDARDS DEPARTMENT OF COMMERCE WASHINGTON, D.C. 20234		7. Contract/Grant No. DE-AT05-800R 206799 AFOSR-ISSA-84-00013 8. Type of Report & Period Covered	
9. SPONSORING ORGANIZATION NAME AND COMPLETE ADDRESS (Street, City, State, ZIP) U.S. Department of Energy AR&TD Fossil Energy Materials Program, Washington, DC 20545 U.S. Air Force Office of Scientific Research, Bldg. 410, Bolling AFB, Washington, DC 20332			
10. SUPPLEMENTARY NOTES <input type="checkbox"/> Document describes a computer program; SF-185, FIPS Software Summary, is attached.			
11. ABSTRACT (A 200-word or less factual summary of most significant information. If document includes a significant bibliography or literature survey, mention it here) Power-law creep parameters of brittle ceramic materials are commonly deduced from load-point displacement data generated by four-point bend experiment, under the assumption that tensile and compressive behaviors obey the same constitutive law. However, thanks to different roles played by microcracking and cavitation, it is now well recognized that this premise on occasions may not be valid. The present paper undertakes an analysis which takes the differences into account. Governing equations are first derived for the locations of neutral axis of a beam under bending and for the creep responses in terms of both curvature rate and load point displacement rate as functions of the applied moment and power-law creep parameters. Numerical solutions are obtained for any given set of materials constants over a wide range of applied moments. It was shown from the plots of creep response versus applied moment on logarithmic scales that nonlinear curves concave upward signify profound difference in stress exponent between tension and compression. An example of applying of the present analysis to a set of load-point displacement data on glass-alumina beam specimens crept at 1100°C is given. The results show that the conventional method over/underestimates the creep rates in compression/tension by two orders of magnitude, indicating a need of undertaking a more accurate analysis. Several recommendations are offered to experimentalists so as to enhance the reliability in the estimation of power-law creep parameters based solely on bend test data.			
12. KEY WORDS (Six to twelve entries; alphabetical order; capitalize only proper names; and separate key words by semicolons) creep analysis; creep of glass alumina; creep of ceramics; creep bend test; four-point bend test; power-law creep			
13. AVAILABILITY <input checked="" type="checkbox"/> Unlimited <input type="checkbox"/> For Official Distribution. Do Not Release to NTIS <input type="checkbox"/> Order From Superintendent of Documents, U.S. Government Printing Office, Washington, D.C. 20402. <input checked="" type="checkbox"/> Order From National Technical Information Service (NTIS), Springfield, VA. 22161		14. NO. OF PRINTED PAGES 43 15. Price \$8.50	

